Acta Radiologica

Draft Manuscript for Review

Perfusion-CT Analysis for assessment of Hepatocellular Carcinoma lesions: Diagnostic Value of Different Perfusion Maps

Journal:	*Acta Radiologica*
Manuscript ID	Draft
Manuscript Type:	Original Article
Keyword:	Abdomen/GI < Areas/Systems, Liver < Structures, Adults < Subject Matter, Cirrhosis < Topics, Hepatocellular Carcinoma, CT-Perfusion

Perfusion-CT Analysis for assessment of Hepatocellular Carcinoma lesions: Diagnostic Value of Different Perfusion Maps

Abstract

Background: CT-liver-perfusion (CTLP) has been improved over the last years, offering a variety of perfusion-parametric-maps. The map that better discriminates hepatocellular carcinoma (HCC) is still to be proven.

Purpose: To compare different CT-liver-perfusion (CTLP) maps, regarding their ability to differentiate cirrhotic or non-cirrhotic parenchyma from malignant hepatocellular carcinoma (HCC).

Material and methods: Twenty-six patients (11 cirrhotic) with 50 diagnosed HCCs, underwent CTLP on a 128-row dual-energy CT-system (Revolution HD,GE,USA). Nine different maps were generated. Regions of interest (ROIs) were positioned on non-tumorous parenchyma and on HCCs found on previous MRI-imaging. Perfusion parameters for non-cirrhotic and cirrhotic livers were compared with Mann-Whitney test. Receiver Operating Characteristic (ROC) analysis was employed to evaluate each map ability to discriminate HCCs from non-tumorous liver. Comparison of ROC curves was performed to evaluate statistical significance of differences in the discriminating efficiency of derived perfusion maps.

Results: Perfusion parameters for non-tumorous liver and HCCs recorded in cirrhotic patients did not significantly differ from corresponding values recorded in non-cirrhotic patients ($p>0.05$). Best parameter for HCC discrimination was MSI, with estimated area under ROC curve of 0.997 and cut-off-criterion 2.2 HU/sec, providing 96% sensitivity and 100% specificity.

Conclusion: MSI perfusion map was found to have the highest power in discriminating HCC nodules from non-tumorous parenchyma. MSI discriminating power did not significantly differ from TTP, whereas differences from all other perfusion parameters were found to be statistically significant.

Keywords

Abdomen/GI < Areas/Systems, Liver < Structures, Adults < Subject Matter, **C**irrhosis < Topics, Hepatocellular Carcinoma, CT-Perfusion

Introduction

Computed tomography liver perfusion (CTLP) examination provides valuable information regarding vascular supply and hepatic tissue characterization (1,2). Acquired data are processed with dedicated vendor-specific-software-packages allowing estimation of CT-perfusion indices regarding quantitative and functional blood flow evaluation (1). Produced quantitative tissue perfusion maps are displayed on color scale permitting tissue perfusion depiction at high spatial resolution and quantification in absolute units. Thus, CTLP enables identification of abnormal tissue areas, which might be difficult to detect with conventional CT-imaging (2,3).

Perfusion maps of quantitative or semi-quantitative parameters, such as blood flow (BF), blood volume (BV), mean transit time (MTT), portal liver perfusion (PLP), arterial liver perfusion (ALP), hepatic perfusion index (HPI) positive enhancement integral (PEI), transit time to impulse residue function peak (Tmax), time to peak (TTP), impulse residue function (IRF-T0), and permeability-surface area product (PS), may be generated by modern CT-systems available in the market (4). The variability in terminology and perfusion parameters adopted by different CT-vendors might cause confusion. The post processing of the attenuation curves is based on different kinetic models and assumptions. Commonly used models are Maximum Slope method (single compartment), Patlak method (double compartment) or deconvolution method.

Regarding hepatocellular carcinoma in cirrhotic or non-cirrhotic patients, there is evidence that CT-perfusion has reached technical maturity allowing reliable assessment of tumor vascularity (5). Some limitations of CTLP technique like breath-holding, of

arterial and portal blood flow separation, radiation exposure, scan range, and standardization of analytic methods should be addressed. Moreover, depending on the main liver disease, some perfusion maps seem to offer more valuable information than others. The motivation of the current study originated from the limited studies existing comparing diagnostic efficiency of available CTLP-maps. The aim of the current study was to compare diagnostic ability of different CTLP-maps in differentiation between liver parenchyma and HCC.

Materials and Methods

Patient cohort

Twenty-six patients (24 male; mean age 73.7 years; range 56-86 years) underwent CTLP in our centre from May-December 2016 (18 Child-Pugh class A, 8 class B). All patients were diagnosed with at least one hepatocellular carcinoma lesion. Eleven patients suffered from cirrhosis (alcoholism in 3, Hepatitis C virus (HCV) infection in 4 cases and Hepatitis B virus (HBV) infection in 4 cases). Percutaneous biopsies were not performed because HCC diagnosis is considered accurate with two non-invasive imaging techniques, if both demonstrate focal lesion >2cm with features of arterial hypervascularization or one single radiologic study combined with a serum AFP level of >400 ng/ml (6)

Baseline inclusion criteria consisted of: 1) patients >18 years; 2) HCC diagnosis made according to EASL radiological or combined criteria (7); 3) no previous systemic HCC treatment; 4) no contraindications to CT-imaging; 5) No portal vein thrombosis or

arterio-portal shunts present on previous imaging; 6) serum creatinine value <1.5 mg/dL. 7) unknown contrast medium allergy.

A total of 50 HCCs (12 in cirrhotic; range 1-7 nodule/patient) were identified. HCCs were confirmed by at least two radiological methods (contrast-enhanced-ultrasound, triple-phase-CT, MRI examination) as mentioned above and associated with presence of typical enhancement findings (arterially enhancing lesion, with washout in venous and late phases) (8). In the follow-up process, all lesions were subsequently confirmed by invasive hepatic angiography.

Before being enrolled, all subjects gave informed consent after the nature of the procedure was explained. This retrospective study was approved by our Hospital's Ethics Committee.

Perfusion CT data acquisition and analysis

All patients were subjected to CTLP examination on a modern 128-slice CT-scanner (Revolution HD, GE Medical Systems, Wisconsin, USA). The volume helical shuttle mode acquisition protocol was employed. CTLP acquisition parameters and contrast media administration protocol are shown in suppl. Table 1. Patients were advised to breathe slowly and shallowly to minimize organ motion during acquisition.

Acquired CT-image datasets were transferred to image analysis server (AW3.2, General Electric, USA) and analyzed using a dedicated image analysis software package (CT-Perfusion-4D, General Electric, USA) which produced various perfusion-related

parameter maps. CT-Perfusion-4D software employs two computational algorithms, a deconvolution-based and a standard algorithm.

The first deconvolves arterial time-density curve from time-density curve of each image voxel to compute an impulse residue function (IRF) from which contrast arrival delay (IRF-T0) and derived perfusion parameters are calculated (Fig. 1). The advantage of deconvolution algorithm over other computational models is that it corrects time delay in the contrast kinetics originating from the non-instantaneous injection rate of the contrast agent. This time delay-corrected algorithm offers a higher immunity to noise, thus a more accurate estimation of IRF-T0. Perfusion map parameters calculated and based on time-delay corrected deconvolution algorithm are listed in suppl. Table 2. The CT-Perfusion-4D software application enables calculation of additional perfusion parameters such as Positive Enhancement Integral (PEI), Time-To-Peak (TTP), and Mean Slope of Increase (MSI) using the "standard" computational model (suppl. Table 2). It is noted that the contrast arrival time delay correction is not implemented in the "standard" computational model.

To compute functional maps for each perfusion-related parameter, a reference arterial input curve was defined by manually drawing a region of interest (ROI) in the aorta and a reference portal vein input was specified by placing a ROI in the portal vein. Color-coded functional maps were generated for all parameters listed in Suppl. Table 2. One special trained Radiologist set the aorta and portal vein ROIs and then analyzed all CTLP-examinations. In HCC lesions detected on color map, a circular or oval ROI was placed within the lesion, in the sections where the tumor had the maximal enhancement; ROIs' sizes were depending on lesions' ROIs delineating HCC nodule(s) were manually

drawn on perfusion maps of each patient with the aid of previous MRI-findings. In addition, a circular ROI was positioned on non-tumorous and non-vascular parenchyma (Fig. 3). Mean values of perfusion parameters were thus derived. No motion correction software was used on the obtained images before creating perfusion maps.

Radiation exposure

Dose-length product (DLP) was recorded for each examination and effective dose to each patient subjected to CTLP was calculated using standard DLP to effective dose conversion coefficient for abdomen k=0.0151 mSv mGy^{-1} cm^{-1} (9).

Statistical analysis

The Mann-Whitney test was employed to compare perfusion parameters of non-tumorous liver parenchyma and HCC, both recorded in non-cirrhotic patients with those corresponding values in cirrhotic patients. ROC analysis was employed to evaluate the potential of each perfusion parameter to discriminate HCC nodules from non-tumorous parenchyma. ROC curves comparison was performed to evaluate statistical significance of differences in the discriminating power of different perfusion maps. A p-value <0.05 was required for a test result to be considered statistically significant. The MedCalc Statistical Software version 15.11.4 (MedCalc Software bvba, Ostend, Belgium) was used.

Results

A total of 50 HCCs were evaluated (mean lesion's diameter 35.2 mm, min 9.0, max 125.0, SD 29.64 mm; median 23.5 mm). Perfusion parameters recorded in non-

tumorous liver parenchyma of non-cirrhotic patients were not found to differ significantly ($p>0.05$) from the corresponding values of cirrhotic patients (Table 1). Parameters recorded for HCCs of non-cirrhotic patients were found similar to those for HCCs of cirrhotic patients ($p>0.05$) (Table 1).

ROC analysis results for all studied perfusion-related parameters and comparison of ROC curves are presented in Table 2. MSI was found to have the highest efficiency to discriminate HCC nodules from non-tumorous liver parenchyma, followed in order by TTP, BF, Tmax, PEI, MTT, HAF, IRF T0, Average, Base and BV (Fig. 2). The discriminating power of TTP was not found to differ significantly from that of MSI ($p>0.05$). All other parameters were found to have significantly lower discriminating ability compared to MSI ($p<0.05$). However, that statistical significance of the differences of BF and Tmax from MSI was marginal. MSI cut-off value, i.e. the criterion for HCC, was found to be 2.2 HU/sec achieving a sensitivity of 96% and a specificity of 100%.

Mean dose length product associated with the employed acquisition protocol was recorded to be 1702 mGy·cm and mean effective dose was estimated to be 25.7 mSv for the acquisition protocol employed.

Discussion

Hepatocellular carcinoma can be found in cirrhotic and non-cirrhotic patients. In non-cirrhotic liver, HCCs are sporadically discovered in relatively elder patients as well-differentiated, usually encapsulated tumors and regular image screening can reduce mortality (10–13). In cirrhotic liver, HCCs are commonly the result of capillarization and

transformation of dysplastic nodules to a poorly-differentiated carcinoma(14,15). Despite some existing limitations, imaging methods like ultrasonography, triple-phase-CT and contrast-enhanced MR-imaging demonstrate high sensitivity and specificity for HCC detection >2 cm in diameter (5,14,16). MR-imaging in particular, has been reported to reach 88% sensitivity and 94% specificity, rates higher than those achieved by multi-phase-CT-imaging (16).

The practice guidelines of the American Association for the Study of Liver Disease (AASLD) define typical HCC as a nodule with arterial hypervascularity and late phase washout compared with liver parenchyma (1). Radiologic staging refers to the imaging-based determination of the number and size of HCC nodules within the liver as well as the presence of macrovascular invasion and extrahepatic metastases (2). Even for diagnosing 1-2 cm HCCs, arterial and delayed CT-phases may provide higher sensitivity than the combination of arterial phase and PVP, and equal performance with triphasic and quadriphasic combinations (3).

Since first CTLP reports, the method has reached technical maturity (4,5) and is nowadays a promising viable biomarker for tumor detection and follow-up (1,17). CTLP is a software-based dynamic CT-technique that evaluates liver's vascular supply and behavior, allowing volumetric imaging calculations and quantitative, functional blood flow evaluation (1,2,14). Considering the time spent for image data analysis, the "standard protocol" offers more rapid calculation in less than 2 minutes time, which is an important factor in daily clinical practice. Apart from being less costly, CTLP is easy to be incorporated into standard protocols, has greater reproducibility and patient acceptability and offers estimation of several perfusion parameters in a single study (18).

In comparison to MR-perfusion, CTLP has several advantages. It has linear relationship between contrast concentration and signal intensity changes, is faster and enables blood flow parameters measurement (1).

Produced by processing of CTLP data, perfusion maps depict quantitative or semi-quantitative perfusion parameters, such as blood flow (BF), blood volume (BV), mean transit time (MTT), hepatic arterial fraction (HAF), transit time to impulse residue function peak (Tmax) and mean slope of increase (MSI) (2,4,19). Nevertheless, the method is not technically homogenized throughout all available CT-systems of different vendors. Therefore, issues regarding standardization, reproducibility and confirmation of perfusion parameters are raised in order to optimize and regulate CTLP (1,4). Each perfusion map has its special characteristics (suppl. Table 2). PEI, TTP and MSI parametric maps are generated using the "standard algorithm". This algorithm assumes that liver tissue constitutes a single-compartment model, where intravenously administered contrast agent is confined to the vascular space alone. This algorithm is computationally simple, generating PEI, TTP and MSI maps within seconds. On the other hand, BF, BV, HAF, Tmax, MTT, and IRF-T0 parametric maps are generated using the "deconvolution algorithm". This algorithm employs a dual-compartment kinetic model, where the intravenously administered contrast agent is assumed to dynamically distribute between vascular and interstitial space in line with the model developed by Johnson-Wilson (20). This algorithm takes into account the time-dependent varying contrast intravascular concentration, originating from the non instantaneous contrast agent injection rate (Fig. 1). Demanding high computational power, the "deconvolution algorithm" requires several minutes to generate the corresponding parametric maps.

The goal of this study was to compare different CTLP-maps, regarding their ability to differentiate HCCs from non-tumorous liver parenchyma. The cohort studied comprised non-cirrhotic and cirrhotic patients. So, the first question was if there is any quantitative difference between normal and cirrhotic liver parenchyma. No statistically significant differences were found ($p>0.05$). These findings may be due to the high number of patients with Child-Pugh class A that we had in our series, and it is well recognized that the functional liver status of class A patients is similar to that of non-cirrhotic liver. The median value (range) of MSI was found to be 0.81 (0.37-2.22) for non-cirrhotic and 0.69 (0.21-1.37) for cirrhotic parenchyma. Therefore the absence of statistically significant differences allowed us to include cirrhotic and non-cirrhotic patients in one single group for studying HCC identification ability of different CTLP maps.

Hypervascular HCCs can be easily detected by CTLP (14), as a "hot-spot" area on perfusion maps. For HCC identification, some maps seem to offer more valuable information than others (21). Hepatic perfusion (HP), arterial perfusion (AP) and hepatic portal index (HPI) have been shown to have the highest sensitivity and specificity to detect viable HCC tissue owing to the vast arterialization of the nodule (22). HP and AP are not available in our software, and thus their evaluation was not possible. Kim et al, found that HPI significantly increases to 86.5% in a HCC nodule compared to adjacent normal liver parenchyma which remains at 14.5% (5). Increase in BF and BV values has been reported to be significant for hypervascular tumors like HCC (4,5,23,24), whereas MTT tends to decrease in areas where arterial-portal shunts are present (4,5). Studying 30 cirrhotic patients, Ippolito et al, found that for every calculated CT perfusion parameter,

there was a significant difference between HCC and background cirrhotic liver (24). More specifically, HP, BV, and AP values were found higher, and TTP lower, in HCCs relative to non-tumorous cirrhotic liver parenchyma. Median parameters values measured within tumor tissue were for HP 45.7 ml/100 g/min, for BV 20.6 ml/100 mg, for AP 44.2 ml/min, and for TTP 18.7 sec (24). The same group confirmed their data later, measuring perfusion (median) values in HCCs to be 45.7-46.3 for HP, 20.4-20.6 for BV, 42.9-44.2 for AP, 75.3% for HPI and 18.7 sec for TTP (14). The corresponding mean perfusion values in cirrhotic liver parenchyma were calculated to be 10.3 for HP, 11.1-11.7 for BV, 10.4-10.9 for AP, 14-17.5 for HPI and 41.7-44.6 for TTP (14,25). Also, Sahani et al reported a significant increase of BF and MTT of HCCs compared to cirrhotic parenchyma (26). Despite our different software package/mathematical model, higher HAF, BF and MSI perfusion values were obtained for HCC lesions compared to non-tumorous liver parenchyma (Table 1). Current findings confirm hypervascular nature of HCC and the typical neo-angiogenesis process of growing neoplastic liver nodules and corroborate the critical role of CT-perfusion as useful non-invasive diagnostic tool for the quantitative assessment of tumor vascularization.

We also tried to evaluate and compare the power of available maps to identify malignant tissue nodules from non-tumorous parenchyma. The parametric map found to better discriminate HCC from non-tumorous liver parenchyma was MSI, followed in order by TTP, BF and Tmax, with an estimated area under ROC curve of 0.997, 0.992, 0.952 and 0.908, respectively (Fig. 2). MSI and TTP maps may be considered equivalent in discriminating HCC from non-tumorous parenchyma since the comparison yielded non-statistically significant difference, while differences between MSI and all other

CTLP-maps were found to be statistically significant. A MSI cut-off-criterion of 2.22 (HU/sec) was found to provide 96% sensitivity and 100% specificity for detecting HCCs.

Although this was not the goal of our study, another question was if perfusion parameters can distinguish different degree of malignancy. Kaufmann et al, did not find any statistical correlation between tumor's size and tumor perfusion magnitude in order to characterize lesions in terms of tumor differentiation (27). While Tsushima et al, reported that well-differentiated HCCs present higher perfusion-values compared to tumors classified at different grade (28). This was also confirmed by Sahani et al, (26). Nevertheless, an optimal quantitative cut-off-value for a proper assessment of degree malignancy, is still unclear and the mentioned studies make a direct comparison of the results not possible. Considering our results, comparisons of studied perfusion parameters between cirrhotic and non-cirrhotic livers yielded no statistical difference for HCCs. If we consider that non-cirrhotic liver HCCs are usually well-differentiated tumors and those in cirrhotic rather poor-differentiated, there was no quantitative difference found between those two. However, comparison with established markers of tumor vascularity or histopathological samples was not performed.

Currently there is no consensus over how to specify the measurement ROI on a HCC nodule (4). We chose to set the HCC ROI into the area of the so-called "maximum intensity", whereas some investigators include the whole suspected tumor area perimeter and others select a spherical area of interest (27). Kaufmann et al tried to find out if the whole volume measurement ROI had any advantage over a ROI set in the maximum perfusion area within the tumor. Best correlation between the two ROIs was found for the BF maps (27). They also showed that by measuring the whole tumor area, the HPI map

correlated well to tumor's differentiation grade, and a HPI of ≥60% was a reliable cut-off between tumor and liver parenchymal arterialization, except for patients with acute portal thrombosis, patients after TIPSS or advanced portal hypertension (27). All three methodologies can be considered as equivalently appropriate till future studies definitely judge on the size, shape and position of ROI delineating the tumor.

The main limitation of the current study is the relatively small number of patients/lesions studied. Further studies with higher patients/lesions numbers are required to confirm current results. Another limitation is that the MSI cut-off-value, determined here, for identifying HCCs, is restricted only to GE-platform users. Namely, the proposed cut-off-value may not be applicable for similar to MSI parametric maps provided by the CTLP processing software package of other vendors.

In conclusion, this study confirms that CT perfusion is reliable and feasible in HCC patients, providing quantitative information about tumor and liver parenchyma vascularization, combined with good anatomic detail in one image. MSI-maps were found to have the highest diagnostic accuracy in discriminating HCCs from non-tumorous parenchyma, closely followed by TTP, BF and Tmax-maps. Moreover, the perfusion parameters of HCCs developed in cirrhotic livers were not found to differ from those of non-cirrhotic patients. Providing morphological as well as quantitative perfusion data, CTLP may be proven useful for detecting HCCs even of small size (≤2 cm).

References

1. Liapi E, Mahesh M, Sahani D V. Is CT perfusion ready for liver cancer treatment evaluation? J Am Coll Radiol 2015;12:111–113.

2. Ogul H, Kantarci M, Genc B, et al. Perfusion CT imaging of the liver: review of clinical applications. Diagnostic Interv Radiol 2014;20:379–389.

3. Kanda T, Yoshikawa T, Ohno Y, et al. Perfusion measurement of the whole upper abdomen of patients with and without liver diseases: Initial experience with 320-detector row CT. Eur J Radiol 2012;81:2470–2475.

4. Miles KA, Lee TY, Goh V, et al. Current status and guidelines for the assessment of tumour vascular support with dynamic contrast-enhanced computed tomography. Eur Radiol 2012;22:1430–1441.

5. Kim SH, Kamaya A, Willmann JK. CT Perfusion of the Liver: Principles and Applications in Oncology. Radiology 2014;272:322–344.

6. Bialecki ES, Di Bisceglie AM. Diagnosis of hepatocellular carcinoma. *HPB* 2005;7:26–34.

7. Bruix J, Sherman M, Llovet JM, et al. Clinical management of hepatocellular carcinoma. Conclusions of the barcelona-2000 EASL conference. In: Journal of Hepatology:421–430.

8. Liver EA for the S of the, Cancer EO for R and T of. EASL–EORTC Clinical Practice Guidelines: Management of hepatocellular carcinoma. J Hepatol 2012;56:908–943.

9. Deak PD, Smal Y, Kalender WA. Multisection CT Protocols: Sex- and Age-specific Conversion Factors Used to Determine Effective Dose from Dose-Length Product1. Radiology 2010;257:158–166.

10. Yasui K, Hashimoto E, Tokushige K, et al. Clinical and pathological progression of non-alcoholic steatohepatitis to hepatocellular carcinoma. Hepatol Res 2012;42:767–773.

11. Trinchet JC. Hepatocellular carcinoma in 2014: Current situation and future prospects. Diagn Interv Imaging 2014;95:705–708.

12. Ascha MS, Hanouneh IA, Lopez R, et al. The incidence and risk factors of hepatocellular carcinoma in patients with nonalcoholic steatohepatitis. Hepatology 2010;51:1972–1978.

13. Zhang B-H, Yang B-H, Tang Z-Y. Randomized controlled trial of screening for hepatocellular carcinoma. J Cancer Res Clin Oncol 2004;130:417–422.

14. Ippolito D, Capraro C, Casiraghi A, et al. Quantitative assessment of tumour associated neovascularisation in patients with liver cirrhosis and hepatocellular carcinoma: Role of dynamic-CT perfusion imaging. Eur Radiol 2012;22:803–811.

15. Park YN, Yang CP, Fernandez GJ, et al. Neoangiogenesis and sinusoidal "capillarization" in dysplastic nodules of the liver. Am J Surg Pathol 1998;22:656–62.

16. Lee YJ, Lee JSJM, Lee JSJM, et al. Hepatocellular Carcinoma: Diagnostic Performance of Multidetector CT and MR Imaging-A Systematic Review and Meta-Analysis. Radiology 2015;275:97–109.

17. Goh V, Ng QS, Miles K. Computed Tomography Perfusion Imaging for Therapeutic Assessment. Has It Come of Age as a Biomarker in Oncology? Invest Radiol 2012;47:2–4.

18. Miles KA, Griffiths MR. Perfusion CT: A worthwhile enhancement? *British Journal of Radiology* 2003;76:220–231.

19. Chen G. Computed tomography perfusion in evaluating the therapeutic effect of transarterial chemoembolization for hepatocellular carcinoma. World J Gastroenterol 2008;14:5738.

20. Lee T-Y, G Purdie T, Stewart E. CT imaging of angiogenesis. 2003.

21. Fischer MA, Kartalis N, Grigoriadis A, et al. Perfusion computed tomography for detection of hepatocellular carcinoma in patients with liver cirrhosis. Eur Radiol 2015;25:3123–3132.

22. Ippolito D, Bonaffini PA, Ratti L, et al. Hepatocellular carcinoma treated with transarterial chemoembolization: Dynamic perfusion-CT in the assessment of residual tumor. World J Gastroenterol 2010;16:5993–6000.

23. García-Figueiras R, Goh VJ, Padhani AR, et al. CT Perfusion in Oncologic Imaging: A Useful Tool? Am J Roentgenol 2013;200:8–19.

24. Ippolito D, Sironi S, Pozzi M, et al. Perfusion Computed Tomographic Assessment of Early Hepatocellular Carcinoma in Cirrhotic Liver Disease. J Comput Assist Tomogr 2008;32:855–858.

25. Ippolito D, Sironi S, Pozzi M, et al. Perfusion CT in cirrhotic patients with early stage hepatocellular carcinoma: assessment of tumor-related vascularization. Eur J Radiol 2010;73:148–52.

26. Sahani D V., Holalkere N-S, Mueller PR, et al. Advanced Hepatocellular Carcinoma: CT Perfusion of Liver and Tumor Tissue—Initial Experience [1]. Radiology 2007;243:736–743.

27. Kaufmann S, Horger T, Oelker A, et al. Characterization of hepatocellular carcinoma (HCC) lesions using a novel CT-based volume perfusion (VPCT) technique. Eur J Radiol 2015;84:1029–1035.

28. Tsushima Y, Funabasama S, Aoki J, et al. Quantitative perfusion map of malignant liver tumors, created from dynamic computed tomography data. Acad Radiol 2004;11:215–23.

Tables

Table 1. Comparison of perfusion parameters between non-cirrhotic and cirrhotic patients [median (range)] for both, non-tumorous parenchyma and HCC nodules.

	Parenchyma			HCC nodule		
	Non-Cirrhotic	**Cirrhotic**	**p**	**Non-Cirrhotic**	**Cirrhotic**	**p**
Average	83 (47-116)	77 (42-87)	0.51	94 (57-169)	99 (56-119)	0.91
Base	63 (36-72)	61 (41-71)	0.86	55 (32-93)	50 (7-61)	0.17
BF	81 (39-153)	60 (27-94)	0.52	179 (71-595)	169 (43-636)	0.71
BV	21 (9-32)	15 (3-27)	0.13	20 (7-58)	22 (10-70)	0.32
HAF	0.24 (0.03-0.86)	0.23 (0.01-0.73)	0.59	0.79 (0.09-0.99)	0.66 (0.26-0.97)	0.84
IRF T0	3.7 (1.0-9.2)	3.7 (0.5-7.1)	0.90	1.8 (0.4-8.4)	1.1 (0.3-4.5)	0.10
MSI	0.81 (0.37-2.22)	0.69 (0.21-1.37)	0.34	4.4(1.9-8.4)	4.2 (1.3-7.5)	0.87
MTT	18 (8-36)	23 (2-29)	0.90	9 (2-16)	10 (4-25)	0.35
PEI	0.15 (0.01-0.40)	0.12 (0.002-0.37)	0.26	0.31 (0.17-0.51)	0.35 (0.09-1.0)	0.27
Tmax	14 (7-21)	15 (2-19)	0.94	6.1 (2.8-13.9)	6.1 (2.6-14.6)	0.73
TTP	46 (28-67)	50 (26-71)	0.29	18 (11-32)	20 (11-40)	0.23

Table 2 ROC analysis of perfusion parameters in descending order regarding the power to discriminate HCC nodules from non-tumorous liver parenchyma.

	ROC analysis					Comparison to MSI ROC curve
	AUC	**p**	**Sensitivity (%)**	**Specificity (%)**	**Cut off value****	**p**
MSI	0,997	<0.0001*	96	100	2.2	-
TTP	0,992	<0.0001*	92	100	25	0.392
BF	0,952	<0.0001*	92	96	108	0.046*
Tmax	0,908	<0.0001*	94	88	10	0.049*
PEI	0,903	<0.0001*	96	77	0.18	0.018*
MTT	0,858	<0.0001*	88	81	14	0.0010*
HAF	0,842	<0.0001*	92	65	0.36	0.0009*
IRF-T0	0,802	<0.0001*	82	69	2.7	0.0004*
Average	0,786	<0.0001*	64	92	88	0.0001*
Base	0,703	0.0036*	92	54	61	<0.001*
BV	0,583	0.219	24	96	31	<0.001*

AUC: area under ROC curve, *statistical significant (p<0.05), ** the units of each parameter are those shown in suppl. Table 2.

Figure Legents

Fig. 1

A schematic diagram of the time delay-corrected impulse residue function (IRF T0) generated through the "CT Perfusion 4D" deconvolution computational model to compute liver perfusion map parameters.

Fig. 2

ROC curves for MSI, TTP, BF, Tmax, PEI and MTT. Circular dots represent the cut-off value of the parameter which provides the highest diagnostic efficiency in discriminating HCC nodules from non-tumorous parenchyma.

Fig. 3

An example of how four different maps (MSI, TTP, Blood Flow and Tmax) demonstrate normal and tumorous parenchyma. On each image, a measuring ROI on exact the same location is set, ROI 3 on an HCC tumor and ROI 4 on normal liver parenchyma.

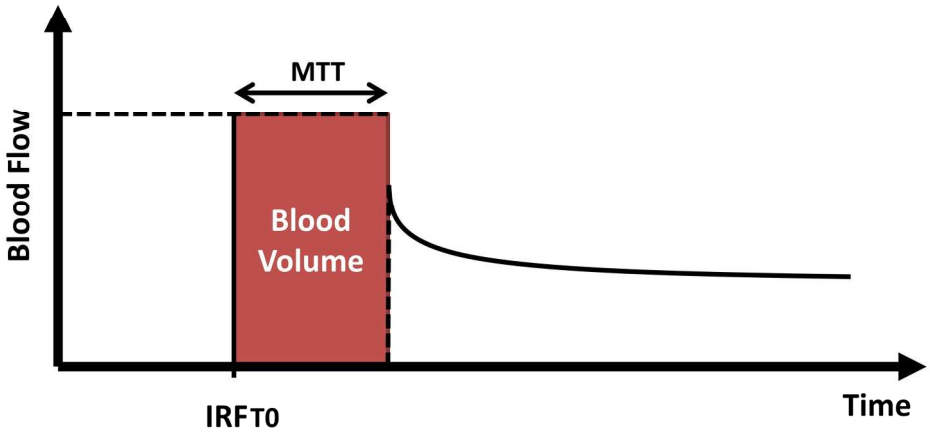

A schematic diagram of the time delay-corrected impulse residue function (IRF T0) generated through the "CT Perfusion 4D" deconvolution computational model to compute liver perfusion map parameters.

95x53mm (600 x 600 DPI)

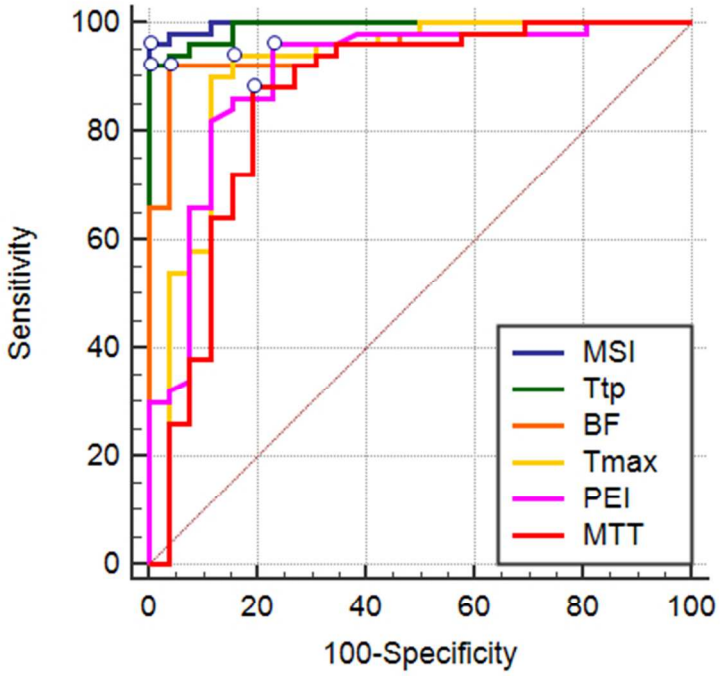

ROC curves for MSI, TTP, BF, Tmax, PEI and MTT. Circular dots represent the cut-off value of the parameter which provides the highest diagnostic efficiency in discriminating HCC nodules from non-tumorous parenchyma.

50x38mm (300 x 300 DPI)

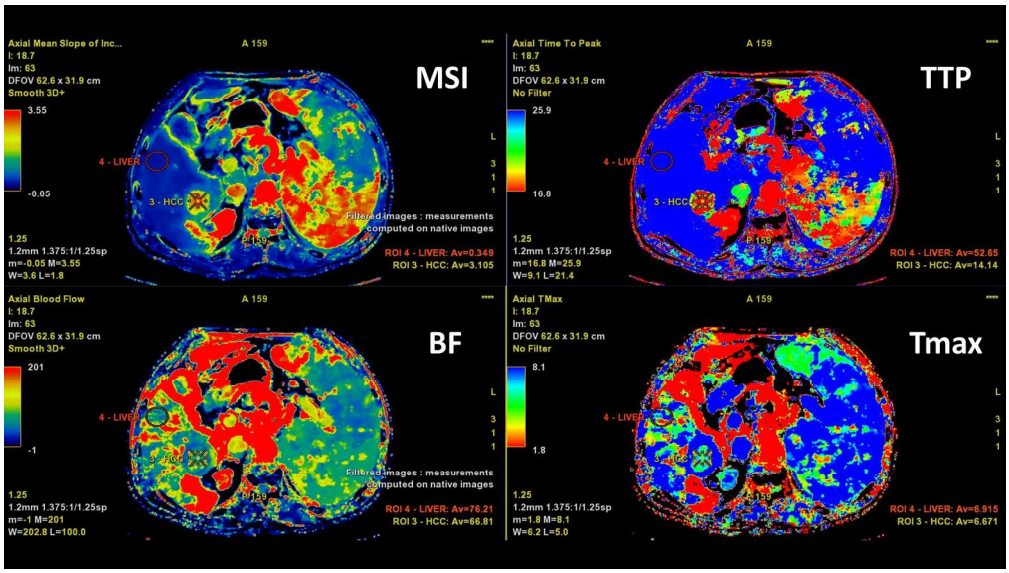

An example of how four different maps (MSI, TTP, Blood Flow and Tmax) demonstrate normal and tumorous parenchyma. On each image, a measuring ROI on exact the same location is set, ROI 3 on an HCC tumor and ROI 4 on normal liver parenchyma.

95x53mm (600 x 600 DPI)

Supplementary Table 1. Perfusion CT acquisition and contrast injection parameters

Parameter	
Tube voltage (kVp)	100
Tube current (mA)	150
Scan length (cm)	14
Scan delay (sec)	5
Number of passes	35
Pass duration (s)	1.7
Total examination time (sec)	59
Reconstructed slice width (mm)	5/1.25
Adaptive Statistical Iterative Reconstruction (%)	40
Iodine administered (ml)	50
Iodine concentration (mg I/ml)	370
Iodine injection rate (ml/sec)	4
Dose length product (mGy x cm) (mean)	1702
Effective Dose (mSv) (mean)	25.7*

*Effective dose was calculated using the standard conversion coefficient for abdomen k=0.0151 (mSv mGy^{-1} cm^{-1}) (6)

Supplementary Table 2. The liver perfusion parameters computed using the deconvolution and the standard computational models.

	Parameter	Definition	Unit
Deconvolution Algorithm	Contrast arrival delay, Impulse residue function to 0 (IRF-T0)	It represents the time of arrival of the contrast agent to a given location and is marked by the onset of tissue enhancement relative to the input artery.	sec
	Blood Flow (BF)	It is estimated as the value of IRF at IRF T0. It is displayed in ml per 100 g of wet tissue per minute.	ml/min/100 g
	Mean Transit Time (MTT)	It is the average residence time of contrast agent in a given tissue location.	sec
	Transit time to impulse residue function peak (Tmax)	It is computed as the time to the peak of the IRF. Tmax = (MTT/2) + IRF T0	sec
	Blood Volume (BV)	It is computed as the product of BF and MTT. It is displayed in ml per 100g of wet tissue. BV = BF x MTT	ml/100 g
	Hepatic arterial fraction (HAF)	It represents the liver blood input contributed by the hepatic artery, as a fraction of the total blood volume. HAF is displayed as a fractional value between 0 and 1.	%
Standard Algorithm	Positive Enhancement Integral (PEI)	It is computed as the area under thetissue density curve in each tissue voxel, divided by the area under the curveof the reference vein ROI.The PEI is displayed as a fractional value between 0 and 1.	%
	Time-to-Peak (TTP)	It is defined as the time interval between the onset of the tissue enhancement and the peak of the tissue density curve. It is computed as the time interval between the last pre-enhancement image and the image with the maximum intensity value.	sec

Mean Slope of Increase (MSI)	It is computed as the average value of the slope function, which is estimated from the tissue density curve for each tissue voxel. The slope function, i.e. s(i+1)-s(i), involves a "running" slope computation for each consecutive pair of time points. $$MSI = \frac{1}{N}\sum_{i=0}^{N-1} s(i+1) - s(i)$$, where, i is the time index and s(i) is the tissue density curve of interest.	Hounsfield unit (HU)/sec